ELSEVIER

Biophysical Chemistry 84 (2000) 159–166

Biophysical Chemistry

www.elsevier.nl/locate/bpc

Detection of the metastable rippled gel phase in hydrated phosphatidylcholine by fluorescence spectroscopy

R. Vladkova[a,*], K. Teuchner[b], D. Leupold[b], R. Koynova[a], B. Tenchov[a]

[a] *Institute of Biophysics, Bulgarian Academy of Sciences, Acad. G. Bonchev St., Bl. 21, 1113 Sofia, Bulgaria*
[b] *Max-Born-Institut für Nichtlineare Optik und Kurzzeitspektroskopie, Rudower Chaussee 6, D-12489 Berlin, Germany*

Received 7 October 1999; received in revised form 22 December 1999; accepted 24 December 1999

Abstract

Steady-state and time-resolved emission spectroscopy of 1-anilinonaphthalene-8-sulfonic acid (ANS) have been used for characterization of the metastable rippled gel phase, P_{β}'(mst), formed in fully-hydrated dipalmitoylphosphatidylcholine (DPPC) upon cooling from the liquid crystalline phase L_{α} [Tenchov et al., Biophys. J. 56 (1989) 757]. The P_{β}'(mst) phase of DPPC clearly differs from the stable P_{β}' phase by increased ($\approx 27\%$) ANS emission intensity, by enhanced ($\approx 23\%$) average radiative rate constant, and by reduced ($\approx 18\%$) non-radiative quenching rate constant. The fluorescence intensity peak at the $P_{\beta}' \rightarrow L_{\alpha}$ transition temperature is replaced by a large, reversible stepwise intensity drop at the P_{β}'(mst) $\rightarrow L_{\alpha}$ transition. No such effects have been found for dimiristoylphosphatidylcholine (DMPC) dispersions confirming previous results that DMPC does not form a P_{β}'(mst) phase. Since ANS is known to predominantly reside in the interfacial region, the observed effects indicate differences between the stable and metastable rippled phases in the organization and dynamics of their lipid/water interfaces. The data demonstrate that the metastable rippled phase manifests its appearance also through interactions with small molecules (ANS size ~ 8 Å).

Keywords: Phase transition; Phospholipid; Polymorphism; Lipid bilayer; ANS; Time-resolved emission spectroscopy

* Corresponding author. Tel.: +359-2-9793694; fax: +359-2-9712493.
E-mail address: vladkova@obzor.bio21.bas.bg (R. Vladkova)

0301-4622/00/$ - see front matter
PII: S0301-4622(00)00107-1

1. Introduction

Saturated diacyl phosphatidylcholines (PC) with fatty acyl chains 15–22 carbons long are characterized by a rich polymorphism (for a review, see [1]). Following low-temperature equilibration, these lipids form lamellar crystalline (subgel) L_c phase which transforms upon heating to a lamellar gel phase (L_β'), and at higher temperature, the so called pretransition takes place — the L_β' phase transforms into the rippled gel phase P_β'. The properties of the latter phase and the physical reasons leading to its formation have been the subject of numerous investigations [2–13]. Upon further heating, the P_β' phase undergoes a highly cooperative melting transition into the lamellar liquid crystalline L_α phase (also called main or chain order/disorder transition). Cooling from the L_α phase of fully hydrated dipalmitoylphosphatidylcholine (DPPC) does not result in the recovery of the P_β' phase but, instead, a metastable rippled phase P_β'(mst) forms [8]. This phase is long-lived at temperatures between the pretransition and the main transition but it readily converts to the initial P_β' phase upon cooling to the L_β' phase and subsequent reheating through the pretransition. High-resolution X-ray scattering data demonstrate that two ripple structures form upon cooling from the L_α phase — a primary one coinciding with that of the stable P_β' phase, with ripple wavelength of 13 nm, and a secondary one with doubled ripple wavelength of 26 nm [9–11]. Such double-period ripple structures have been observed by freeze-fracture electron microscopy as well [5,13]. It has recently been shown that metastable rippled phases also form in distearoylphosphatidylcholine (DSPC) and dihexadecylphosphatidylcholine (DHPC) but not in dimiristoylphosphatidylcholine (DMPC), a saturated PC with long chains of 14 C-atoms [12]. The thermodynamic parameters of P_β'(mst) in DPPC, DSPC and DHPC have been characterized in detail by means of differential scanning calorimetry (DSC) and scanning densitometry. However, P_β'(mst) could not be detected by the latter two methods in DMPC dispersions.

In the present work, we used steady-state and time-resolved emission spectroscopy of a fluorescent probe, ANS, to characterize the differences between the P_β' and P_β'(mst) phases. A number of fluorescence parameters turned out to have substantially different values between the stable and metastable rippled phases of fully hydrated DPPC suspensions. Since ANS is known to be localized at the membrane/water interface, these differences should be interpreted in terms of interactions involving the lipid headgroups and interfacial water. No such effects have been detected for DMPC dispersions.

2. Materials and methods

2.1. Sample preparation

1,2-Dimyristoyl-*sn*-glycero-3-phosphocholine (DMPC), 1,2-dipalmitoyl-*sn*-glycero-3-phosphocholine (DPPC) and the fluorescent probe, 1-anilinonaphthalene-8-sulfonic acid magnesium salt (ANS) were purchased from Fluka, Basel. Water was quartz-bidistilled and de-ionized (pH = 5.2, conductivity $\sigma < 0.1$ μS cm^{-1}). Multilamellar lipid vesicles (MLV) were prepared by dispersing lipid in required amounts of water containing 5 μM dissolved ANS. The lipid concentration was constant (1 mM) in all preparations and the lipid/probe ratio was 200:1, substantially below the binding capacities of these membranes for ANS [14]. The dispersions were incubated at temperature 10°C above the main transition for 30 min and then vortex-mixed 10 times at these temperatures for 15 s over a 30-min period. The samples were slowly cooled through the transition range over the course of 40–50 min and kept overnight for full hydration. The MLV dimensions examined by light microscopy were 0.5–30 μm, with approximately 80% of them in the range 5–15 μm.

2.2. Instrumentation and measuring procedure

Calorimetric measurements were performed using a high-sensitivity differential adiabatic scanning microcalorimeter DASM-4 (Biopribor, Pushchino) as described by Koynova et al. [12]. Absorption spectra were recorded on a LAM-

BDA-19 spectrometer (Perkin Elmer). Quantum proportionally corrected steady-state fluorescence spectra were measured with a FLUOROLOG FL-112 (Instruments S.A.) in front face fluorescence detection mode. The excitation wavelength was 337 nm.

The measurement of the fluorescence decays was carried out using a previously described apparatus [15]. A nitrogen laser MSG 850 (LTB Berlin; $\lambda_{exc} = 337.1$ nm, pulse duration ≈ 500 ps) was used as excitation source and a photomultiplier with boxcar integrator as detection system. The fluorescence decays were registered at 10 wavelengths in the 440–570-nm range by using a monochromator (aperture $f/3$, spectral bandwidth ≈ 1 nm). The decay curves were deconvoluted from the excitation laser pulse using the global analysis method [16], as described in [17]. The true decay functions were simulated as sums of up to three exponentials. The calculated parameters were used to reconstruct the time-resolved emission spectra.

In both cases (steady-state and time-resolved fluorescence measurements) the sample holder was temperature controlled (4–62°C) using Peltier elements. The sample temperature was monitored by a high-precision temperature measuring instrument P550 (Dostmann electronic; temperature resolution better than 0.02°C) inserted in the sample cell (a cuvette with an optical pathlength of 1 cm was used) and positioned just above the irradiated sample area. The samples were magnetically stirred throughout the experiments. The temperature was changed with a rate of less than 0.5°C min^{-1} between the measurements. At each temperature the sample was equilibrated 8–13 min before measurement. Inspection of the temperature in the cuvette volume showed the absence of noticeable temperature gradients.

3. Results and discussion

3.1. Differential scanning calorimetry and steady-state fluorescence spectroscopy

As reported in a previous work [12], the formation of the metastable rippled phase P_{β}'(mst) is detectable by DSC. It is reflected as differences in the thermodynamic characteristics of the $P_{\beta}' \rightarrow L_{\alpha}$ and $P_{\beta}'(mst) \rightarrow L_{\alpha}$ transition peaks, mostly the transition temperature T_m and the maximum heat capacity C_p^{max}. For DPPC, T_m of the $P_{\beta}'(mst) \rightarrow L_{\alpha}$ transition is 0.06°C lower and C_p^{max} is 3 kcal K^{-1} mol^{-1} lower as compared to those for the $P_{\beta}' \rightarrow L_{\alpha}$ transition [12]. For DMPC, such differences were not observed. Here we checked by DSC whether the presence of the fluorescence probe ANS at the quantities applied for the fluorescence measurements would affect the formation of P_{β}'(mst). As seen from the thermograms in Fig. 1a, ANS does not prevent the formation of the metastable rippled phase in DPPC. The T_m for the $P_{\beta}'(mst) \rightarrow L_{\alpha}$ transition in the DPPC + ANS system is 0.07°C lower as compared to the $P_{\beta}' \rightarrow L_{\alpha}$ transition. The maximum heat capacity of that transition is also some 1–2 kcal K^{-1} mol^{-1} lower. The minor differences in the transition characteristics due to the presence of ANS consist of the increased transition temperatures [cf. 41.56°C and 41.49°C for the $P_{\beta}' \rightarrow L_{\alpha}$ and $P_{\beta}'(mst) \rightarrow L_{\alpha}$ transition, respectively, in the presence of ANS, with 41.47° and 41.41°C without ANS] and the slightly increased transition halfwidth by approximately 0.06–0.08°C. Based on these data, we conclude that, in the presence of ANS at lipid/probe molar ratio of 200:1, DPPC still forms P_{β}'(mst) while DMPC still does not.

Fig. 2 shows the integral steady-state fluorescence intensity of ANS in DMPC and DPPC during heating to L_{α} phase and subsequent cooling to 18 and 37°C, respectively. Similar curves were obtained also with the maximum fluorescence at 480 nm plotted as function of temperature. The temperature profiles in Fig. 2 clearly exhibit the lamellar gel → rippled gel ($L_{\beta}' \rightarrow P_{\beta}'$) and rippled gel → lamellar liquid crystalline ($P_{\beta}' \rightarrow L_{\alpha}$) phase transitions at temperatures close to the transition temperatures recorded by DSC. The fluorescence increase at both the pre- and main phase transitions should be attributed to the appearance of additional binding sites for ANS in the phase coexistence regions. Similar maxima in ANS binding and transport through phospholipid bilayers in the main transition region have been reported earlier [18,19]. It is seen however from

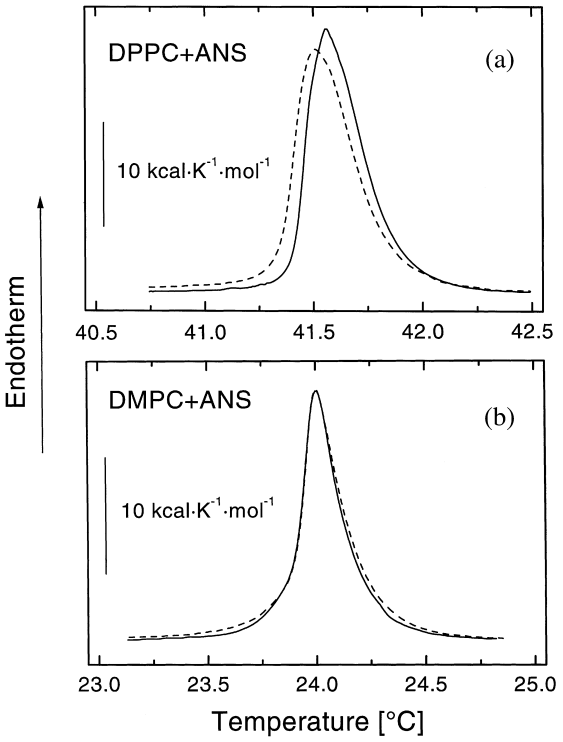

Fig. 1. DSC heating thermograms for fully hydrated dispersions of (a) DPPC (1 mM) + 5 μM ANS, recorded after cooling from 45°C to 20°C (full line) and to 35°C (dashed line), and (b) DMPC (1 mM) + 5 μM ANS recorded after cooling from 28°C to 10°C (full line) and to 17°C (dashed line). Heating rate 0.5°C min^{-1}.

Fig. 2a that upon cooling from L_α through the main transition leading to formation of the metastable rippled phase, the emission peak found in heating direction is replaced by a large stepwise increase of the emission intensity. At 38°C the total intensity is approximately 27% higher than that for the stable rippled phase. This stepwise intensity change is fully reversible — subsequent heating curves from P_β'(mst) phase of DPPC virtually coincide with the cooling one. No such behavior has been observed for DMPC. In that case, an emission peak at the main transition is observable in both heating and cooling directions and cooling results in much smaller, within the error limits, intensity increase for the rippled phase (Fig. 2b). The temperature dependence of the ANS fluorescence confirms the previously reported peculiarities of the P_β'(mst) phase [8,9,12].

This phase is relatively long-lived — incubation for 17 h at a constant temperature of 38°C does not affect the fluorescence intensity shown in Fig. 2a, while, on the other hand, the intensity values typical of the initial P_β' phase readily recover after cooling to the L_β' phase and reheating through the pretransition. No changes in the peak position and halfwidth of the steady-state ANS emission spectra for both lipids have been observed during heating, cooling and second heating runs (data not shown). It thus appears that the latter two parameters are not sensitive to the difference between stable and metastable rippled phases of DPPC. These data represent the first demonstration that the metastable rippled phase manifests its appearance also through interactions with small probe molecules (ANS dimension ~ 8 Å). Since ANS in lipid bilayers is known to be localized in the vicinity of the lipid glycerol back-

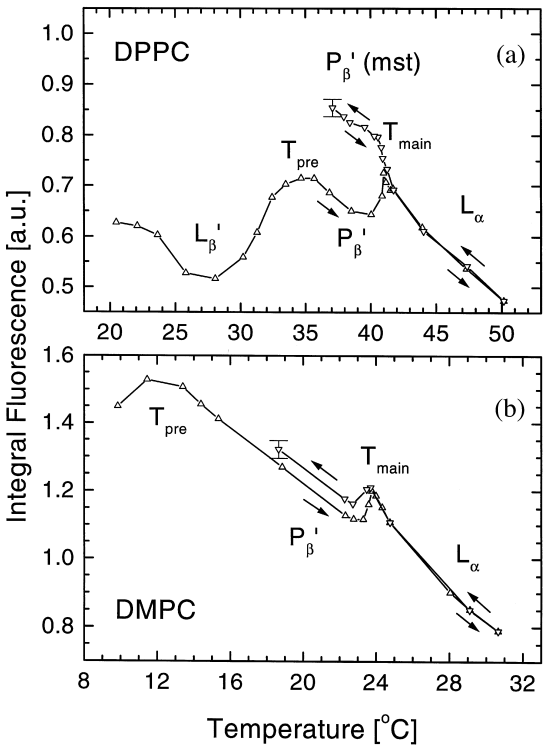

Fig. 2. Integral steady-state fluorescence intensity of ANS in DPPC (a) and DMPC (b) dispersions in water during heating to L_α phase temperatures (– △ – △ –) and subsequent cooling to 37 and 18°C (– ▽ – ▽ –), respectively.

bone (for a review, see Slavik [20]), one may expect that the properties of the lipid/water interface in the metastable phase considerably differ from those in the stable one. The much higher fluorescence intensity in P_β'(mst) may result from ANS redistribution from the water phase (quantum yield, 0.004 [20]) into the lipid phase as well as from enhanced quantum yield of the bound ANS molecules. In an attempt to assess the contribution of these factors, a time-resolved emission spectroscopy characterization of these two phases was carried out.

3.2. Time-resolved emission spectra

Fluorescence decay curves at 10 wavelengths in the 440–570-nm range were recorded at 38°C in the stable and metastable rippled P_β' phases. The deconvolution of these curves was carried out using the global analysis approach. For both phases, best fits were obtained for three exponential decays. The exponential amplitudes, a_i, and the amplitude-averaged relaxation times, $\langle\tau_f\rangle = (\Sigma a_i \cdot \tau_i)/(\Sigma a_i)$, are given as functions of wavelength in Fig. 3a,b, respectively. As is evident from Fig. 3a, the fast component a_1 is much better expressed at shorter wavelengths and gradually decreases to zero with increase of wavelength. The higher a_1 values at shorter wavelengths which are due, in principle, to emission from non-equilibrated ANS excited states contribute to a significant decrease of $\langle\tau_f\rangle$ for wavelengths < 520 nm (Fig. 3b). The $a_1(\lambda)$ dependence for the stable rippled phase also indicates a contribution from ANS emission in water (emission maximum at 515–520 nm) which is absent in the metastable phase.

Sequences of time-resolved emission spectra (TRES) reconstructed from the parameters in Fig. 3 are shown in Fig. 4. Their intensity for the metastable phase is higher, in fairly good agreement with the steady-state fluorescence measurements. For example, the spectra area ratio at time zero $I_{mst}(t=0)/I_{st}(t=0)$ is 1.17 while the ratio of the total TRES intensities integrated up to 50 ns is 1.26. Several initial TRES from the P_β'(mst) phase display well-resolved splitting, most likely due to the more heterogeneous environment that

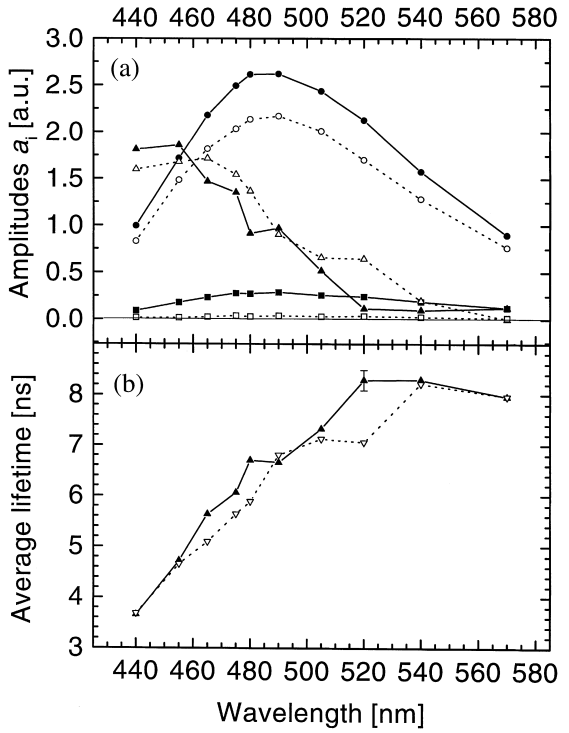

Fig. 3. (a) Pre-exponential amplitudes a_1 (triangles), a_2 (circles), a_3 (squares); and (b) amplitude-average fluorescence lifetimes $\langle\tau_f\rangle$ of ANS in the stable (open symbols) and metastable (solid symbols) rippled phases of fully hydrated DPPC at 38°C. (a) Decay times for the stable phase: $\tau_1 = 0.7$ ns, $\tau_2 = 8.7$ ns, $\tau_3 = 46.1$ ns; for the metastable phase: $\tau_1 = 0.8$ ns, $\tau_2 = 7.6$ ns, $\tau_3 = 17.7$ ns.

this phase creates for ANS by the appearance of the secondary ripple structure in coexistence with the primary one [9,10]. The differences between the TRES profiles of the P_β' and P_β'(mst) phases display at times up to approximately 2.6 ns after excitation and smear out at longer times. The contribution of this short-lived emission to the time-integrated TRES is however only 3–4%, thus rendering these differences unobservable in the steady-state fluorescence spectra of the two phases. With increase of time after the excitation, the emission maxima experience a red shift in both rippled phases. Similar red shifts have also been observed for a number of other lipid/fluorescent probe systems [20–22]. Such shifts in the nanosecond range are frequently ascribed to reorientation and equilibration of the lipid dipoles

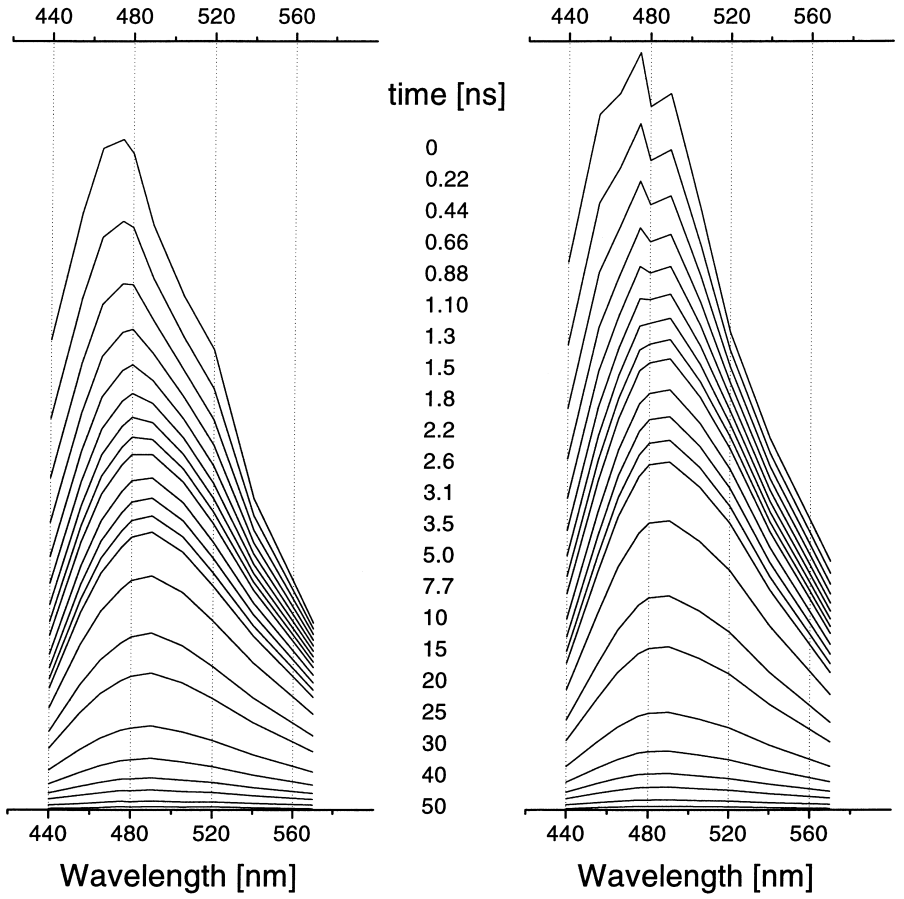

Fig. 4. Time-resolved emission spectra of ANS in DPPC at 38°C in the stable (left) and in the metastable (right) P_{β}' phases. The times after excitation for these spectra are given in the middle.

surrounding the excited-state dipole of the probe molecule.

Since the initial fluorescence intensity at $t = 0$ is inversely proportional to the radiative lifetime τ_r, the intensity difference between the two rippled phases may be considered as due to a reduced τ_r of ANS in the metastable phase. For a single lifetime emission, τ_r can be obtained from the relations $k_r = 1/\tau_r = \phi/\tau_f$ and $\tau_f = 1/(k_{nr} + k_r)$, where ϕ is the quantum yield, k_{nr} and k_r are the non-radiative and radiative rate constants, respectively. For multiexponential emission decays, amplitude-averaged lifetimes $\langle \tau_f \rangle$ should be used [23,24]. Since $\langle \tau_f \rangle$ changes with the wavelength (Fig. 3b) while the radiative rate constants are λ-independent, amplitude fractions α_i that are independent of wavelength have to be introduced. Following [24], $\alpha_i = [\int a_i(\lambda)\mathrm{d}\lambda]/[\int \Sigma a_i(\lambda)\mathrm{d}\lambda]$; $\langle k_r \rangle = \phi/\Sigma\alpha_i\tau_i$, where $\langle k_r \rangle$ is the absorption weighted average k_r and $\Sigma\alpha_i\tau_i$ is the λ-independent amplitude-averaged fluorescence lifetime. Thus determined lifetime values are 6.3 ns and 6.6 ns for the stable and the metastable phases, respectively. Using these values and a quantum yields ratio determined as ratio of the total nanosecond emission ($\phi_{\mathrm{mst}}/\phi_{\mathrm{st}} = 1.26$), we obtain $\langle \tau_r \rangle_{\mathrm{st}} = 1.20 \times \langle \tau_r \rangle_{\mathrm{mst}}$. This ratio is close to $[I_{\mathrm{mst}}(t = 0)/I_{\mathrm{st}}(t = 0)] = 1.17$ thus providing an argument that the enhanced initial TRES intensity of the metastable phase results from a reduced radiative time. Since specific interactions between ANS and water are known to increase

τ_r[20,25,26], the above estimates indicate suppressed water access to ANS in the P_β'(mst) phase, either due to ANS molecules additionally bound to the lipid phase, or to better shielding of its interactions with interbilayer water. Such a conclusion is also supported by the absence of ANS emission in water in the case of the metastable phase (Fig. 3a). If we use the quantum yield value $\phi = 0.24$ for ANS in DPPC at 30°C [14] as a reference, the quantum yields for the stable and metastable rippled phases at 38°C could be estimated as 0.28 and 0.36, respectively. Using these values, and the relation $k_{nr} = (1 - \phi)/\tau_f$, the average non-radiative quenching rate constants k_{nr} of ANS in the stable and metastable phases become 1.14×10^8 s^{-1} and 0.97×10^8 s^{-1}, respectively. The values of the radiative rate constants for the stable and metastable phases are 0.44×10^8 s^{-1} and 0.54×10^8 s^{-1}, respectively. The ratios k_{nr}/k_r for the stable and metastable phases are 2.6 and 1.8, respectively. Thus, the non-radiative ANS deactivation dominates in both phases but with strongly reduced efficiency (by approx. 44%) in the metastable phase. Based on these estimates, we conclude that the local environment of the excited ANS molecules in the metastable P_β'(mst) phase is characterized, on the average, by a reduced mobility in comparison to the stable P_β' phase. As a word of caution, it is worth noting that this effect might be associated with ANS redistribution from the water into the lipid phase of P_β'(mst) rather than with an intrinsic difference in the lipid dynamics of the two rippled phases.

4. Conclusions

Both the steady-state and time-resolved emission spectra of the fluorescent probe ANS incorporated in fully hydrated DPPC bilayers clearly distinguish between the stable and metastable rippled gel phases of this lipid. ANS parameters sensitive to the formation of the metastable rippled phase are the emission intensity and the average radiative and non-radiative rate constants. An intensity maximum observed at the temperature of the $P_\beta' \rightarrow L_\alpha$ transition is replaced by a large, reversible stepwise intensity variation at the P_β'(mst) $\leftrightarrow L_\alpha$ transition. In contrast to the stable phase, the metastable phase appears to bind more ANS molecules and to provide an environment with reduced ability for fluorescence quenching. The data provide evidence that the metastable and stable rippled phases differ in the organization and dynamics of their lipid/water interfacial layers and that the metastable rippled phase manifests its appearance also through interactions with small molecules.

Acknowledgements

Financial support of this work by the Deutsche Forschungsgemeinschaft (projects 436 BUL 17/1/98 and 436 BUL 112/11/99) and by the Bulgarian Academy of Sciences is gratefully acknowledged.

References

[1] R. Koynova, M. Caffrey, Phases and phase transitions of the phosphatidylcholines, Biochim. Biophys. Acta 1376 (1997) 91–145.
[2] M.J. Janiak, D.M. Small, G.G. Shipley, Nature of the thermal pretransition of synthetic phospholipids: dimyristoyl- and dipalmitoyllecithin, Biochemistry 15 (1976) 4575–4580.
[3] B.R. Lentz, E. Freire, R.L. Biltonen, Fluorescence and calorimetric studies of phase transitions in phosphatidylcholine multilayers: kinetics of the pretransition, Biochemistry 17 (1978) 4475–4480.
[4] D.G. Cameron, H.L. Casal, H.H. Mantsch, Characterization of the pretransition in 1,2-dipalmitoyl-*sn*-glycero-3-phosphocholine by Fourier transform infrared spectroscopy, Biochemistry 19 (1980) 3665–3672.
[5] B.R. Copeland, H.M. McConnell, The rippled structure in bilayer membranes of phosphatidylcholine and binary mixtures of phosphatidylcholine and cholesterol, Biochim. Biophys. Acta 599 (1980) 95–109.
[6] M. Akiyama, Y. Terayama, N. Matsushima, Kinetics of pretransition in multilamellar dimyristoylphosphatidylcholine vesicle. X-Ray diffraction study, Biochim. Biophys. Acta 687 (1982) 337–339.
[7] J.A. Zasadzinski, Effect of stereoconfiguration on ripple phases (P beta′) of dipalmitoylphosphatidylcholine, Biochim. Biophys. Acta 946 (1988) 235–243.
[8] B.G. Tenchov, H. Yao, I. Hatta, Time-resolved X-ray diffraction and calorimetric studies at low scan rates. I.

Fully hydrated dipalmitoylphosphatidylcholine (DPPC) and DPPC/water/ethanol phases, Biophys. J. 56 (1989) 757–768.

[9] H. Yao, S. Matuoka, B. Tenchov, I. Hatta, Metastable ripple phase of fully hydrated dipalmitoylphosphatidylcholine as studied by small angle X-ray scattering, Biophys. J. 59 (1991) 252–255.

[10] S. Matuoka, H. Yao, S. Kato, I. Hatta, Conditions for the appearance of the metastable P_{β}' phase in fully hydrated phosphatidylcholines as studied by small-angle X-ray diffraction, Biophys. J. 64 (1993) 1456–1460.

[11] M. Rappolt, G. Rapp, Structure of the stable and metastable ripple phase of dipalmitoylphosphatidylcholine, Eur. Biophys. J. 24 (1996) 381–386.

[12] R. Koynova, A. Koumanov, B. Tenchov, Metastable rippled gel phase in saturated phosphatidylcholines: calorimetric and densitometric characterization, Biochim. Biophys. Acta 1285 (1996) 101–108.

[13] H.W. Meyer, Pretransition-ripples in bilayers of dipalmitoylphosphatidylcholine: undulation or periodic segments? A freeze-fracture study, Biochim. Biophys. Acta 1302 (1996) 138–144.

[14] D.H. Haynes, H. Staerk, 1-Anilino-8-naphthalenesulfonate: a fluorescent probe of membrane surface structure, composition and mobility, J. Membrane Biol. 17 (1974) 313–340.

[15] K. Teuchner, W. Becker, H. Stiel, Multidecay fluorescence measurements with an extended digital signal sampling device, Meas. Sci. Technol. 4 (1993) 1070–1076.

[16] J.R. Knutson, J.M. Beechem, L. Brand, Simultaneous analysis of multiple fluorescence decay curves: a global approach, Chem. Phys. Lett. 102 (1983) 501–507.

[17] H. Stiel, K. Teuchner, D. Leupold, S. Oberländer, J. Ehlert, R. Jahnke, Computer aided laser-spectroscopic characterization and handling of molecular excited states, Intellig. Instrum. Comput. 9 (1992) 79–88.

[18] T. Tsong, Effect of phase transition on the kinetics of dye transport in phospholipid bilayer structures, Biochemistry 14 (1975) 5409–5414.

[19] K. Jacobson, D. Papahadjopoulos, Effect of a phase transition on the binding of 1-anilino-8-naphthalenesulfonate to phospholipid membranes, Biophys. J. 16 (1976) 549–560.

[20] J. Slavik, Anilinonaphthalene sulfonate as a probe of membrane composition and function, Biochim. Biophys. Acta 694 (1982) 1–25.

[21] T. Parasassi, F. Conti, E. Gratton, Time-resolved fluorescence emission spectra of Laurdan in phospholipid vesicles by multifrequency phase and modulation fluorometry, Cell. Mol. Biol. 32 (1986) 103–108.

[22] A. Sommer, F. Paltauf, A. Hermetter, Dipolar solvent relaxation on a nanosecond time scale in ether phospholipid membranes as determined by multifrequency phase and modulation fluorometry, Biochemistry 29 (1990) 11134–11140.

[23] A.G. Szabo, C. Faereman, Dilemma of correlating fluorescence quantum yields and intensity decay times in single tryptophan mutant proteins, SPIE 1640 (1992) 70–80.

[24] A. Sillen, Y. Engelborghs, The correct use of 'average' fluorescence parameters, Photochem. Photobiol. 67 (1998) 475–486.

[25] G.W. Robinson, R.J. Robbins, G.R. Flemming, J.M. Morris, A.E.W. Knight, R.J.S. Morrison, Picosecond studies of the fluorescence probe molecule 8-anilino-1-naphthalenesulfonic acid, J. Am. Chem. Soc. 100 (1978) 7145–7150.

[26] T.W. Ebbesen, C.A. Ghiron, Role of specific solvation in the fluorescence sensitivity of 1,8-ANS to water, J. Phys. Chem. 93 (1989) 7139–7143.